Research Article | Vol. 29, No. 19 / 13 Sep 2021 / Optics Express 30020
Optics EXPRESS

CDDA: extension and analysis of the discrete dipole approximation for chiral systems

S. A. Rosales,[1] P. Albella,[1] F. González,[1] Y. Gutiérrez,[2] and F. Moreno[1,*]

[1]Group of Optics. Department of Applied Physics Faculty of Sciences. University of Cantabria., 39005 Santander, Cantabria, Spain
[2]Institute of Nanotechnology CNR-NANOTEC, Via Orabona 4, 70126 Bari, Italy
*morenof@unican.es

Abstract: Discrete dipole approximation (DDA) is a computational method broadly used to solve light scattering problems. In this work, we propose an extension of DDA that we call Chiral-DDA (CDDA), to study light-chiral matter interactions with the capability of describing the underlying physics behind. Here, CDDA is used to solve and analyze the interaction of a nanoantenna (either metallic or dielectric) with a chiral molecule located in its near field at different positions. Our method allowed to relate near field interactions with far field spectral response of the system, elucidating the role that the nanoantenna electric and magnetic polarizabilities play in the coupling with a chiral molecule. In general, this is not straightforward with other methods. We believe that CDDA has the potential to help researchers revealing some of the still unclear mechanisms responsible for the chiral signal enhancements induced by nanoantennas.

1. Introduction

The spectroscopic characterization of chiral matter assisted by nanostructures has recently become an active topic [1–28]. There is a special interest in pharmaceutics to distinguish and separate enantiomers of chiral biomolecules for health reasons [29]. One of the main techniques to characterize mixtures of enantiomers is circular dichroism (CD) spectroscopy, that is based on the measurement of the difference between the left and right circularly polarized light (LCPL and RCPL) extinction, or optical rotation (OR) of linearly polarized light [30]. Recently, several works have shown how the CD and OR exhibited by biomolecules can be enhanced by means of interaction with plasmonic or high refractive index (HRI) nanoantennas (NAs) [1–28]. These NAs consist of structures with sizes ranging from ten to a few hundreds of nanometers made of materials with optical properties that enable resonant interaction with light [31–33]. This interaction can result in an enhancement of the electromagnetic field amplitude in the surrounding of the NA and is the basis of many surface-enhanced spectroscopies [21–23,31–37]. In parallel, many chemists and materials scientists have followed on developing techniques that allow the fabrication of many nanostructures involving chiral matter [38,39]. These are key aspects to consider for achieving an industrial capability of the nanomaterial-based chiral matter characterization techniques.

With this experimental scenario, it becomes crucial to have computational methods that provide experimentalists a tool not only to reproduce the experimental results but also to interpret and understand the still unclear origin and the physical mechanisms behind the CD or OR enhancement [1–6,24]. Many theoretical studies focus on optimization of the isolated nanostructures ignoring interactions of those nanostructures with chiral matter [17–20,40]. Other studies explore the interaction of chiral matter with nanostructures by just considering an isotropic layer of material with certain chiral properties surrounding the nanostructure [5–10,23]. Even though this is the most realistic situation, its electromagnetic solution is typically obtained by computational methods such as finite differences in the time domain (FDTD) or any other finite element method

#434061 https://doi.org/10.1364/OE.434061
Journal © 2021 Received 14 Jun 2021; revised 2 Aug 2021; accepted 2 Aug 2021; published 1 Sep 2021

Optics EXPRESS

(FEM), without elucidating the physical origin of CD enhancement. These methods require high-level coding, so in most practical cases researchers end up relying on commercial software. The flexibility of this software is limited by the scarce knowledge and access that the user has to the codes that run the simulation. As a consequence, the simulations consist of a closed solution given an input optical signal, ignoring the intermediate interactions responsible for the enhancement. Some attempts to elucidate CD enhancement mechanisms have been done based on approximations like considering the nanostructures as strong dipoles [23–28]. Nevertheless, those studies were only centered in partial results, like molecular absorption obviating the NA scattering contribution to the total extinction [24–28], CD enhancements with the molecule fixed at one position [24], or CD enhancements with metals bypassing HRI dielectric nanostructures [26–28]. To consider the effects that multipolar contributions of the NA have on the optical response of chiral systems, a more complete description has to be considered rather than dipolar approximations. The discrete dipole approximation (DDA), which consists of discretizing the system in a large number of coupled electric dipoles, is a suitable approach to describe the NAs multipolar resonances [41,42].

As far as we are concerned, this is the first time that an extension of the DDA formalism is proposed to numerically solve a light scattering problem where chiral matter is present. In this work, the extension of the DDA to address the interaction of light with nanostructures and chiral matter is introduced. We call it *chiral DDA* (CDDA), because it considers the presence of one or more mixed electric-magnetic polarizabilities, an intrinsic property of chiral molecules. With a DDA formalism is relatively easy to separate the different electromagnetic contributions present in the problem such as the extinction produced by the NA and the chiral molecules or even the individual dipolar resonances of the NA. These specific features facilitate a deep understanding of the NA-molecule interaction at levels that can not be easily reached with other numerical methods like FDTD or FEM. In addition, DDA formalism is easier to handle and implement than FDTD or FEM, with the main drawback of slow convergence [42]. We believe that this novel method can help researchers to reveal some of the still unclear mechanisms responsible for the chiral signal enhancements induced by NAs and boost the design of more efficient chiral sensors.

The manuscript is organized as follows: in section 2 we describe the CDDA method. In section 3, we test CDDA by studying an scattering problem that can also be solved with a particular analytic solution (chiral Mie theory). Section 4 is devoted to showing the novel utility of the CDDA method by solving an interesting situation that has been widely explored experimentally [1,14–16] and not fully explained in other theoretical studies that use other computational tools [5–10,18–20,24–28]. We conclude with section 5 that summarizes the main results of this work and the potential that our method offers.

2. CDDA method

2.1. Coupling between general dipoles

The basic description and mathematical formalism of the DDA method for coupled magnetic-electric dipoles can be found in [43]. In this work, we have slightly changed the notation. As a novelty, here we have incorporated the mixed magnetic-electric polarizability, necessary to account for chiral matter. A typical chiral scatterer, such as a chiral molecule, exhibits an electric and magnetic dipolar moment that depends simultaneously on the electric and magnetic incident field [44]

$$\begin{aligned} \mathbf{p_i} &= \alpha_{e,i}\mathbf{E_i} - i\mu_0 G_i \mathbf{H_i} \\ \mathbf{m_i} &= iG_i\mathbf{E_i} + \alpha_{h,i}\mathbf{H_i} \end{aligned} \tag{1}$$

where i stands for the i-th dipole, $\alpha_{e,i}$ and $\alpha_{h,i}$ are the electric and magnetic dipolar polarizabilities respectively, G_i is the mixed magnetic-electric polarizability and μ_0 is the vacuum permeability. These polarizabilities are in general 3x3 tensors for anisotropic materials, but are proportional to

Optics EXPRESS

the identity matrix for the case of isotropic ones. The method proposed here can be applied to both cases in the same way as DDA [41,42].

It is expected that when a chiral response is considered, i.e. a non zero G_i, the typical DDA problem, where only electric polarizabilities are considered [41,42], is no longer valid. In this case, interactions between electric and magnetic dipoles have to be introduced [43]. To do so, we need to know the electric and magnetic field the j^{th} dipole radiates to the i^{th} dipole,

$$\begin{aligned}\mathbf{E_{si,j}} &= \frac{e^{ikr_{ji}}}{4\pi r_{ji}}\left[\frac{1}{\epsilon_0 n_m^2}\left(A_{ji}\mathbb{I}_3 + B_{ji}\mathbf{n_{ji}}\otimes\mathbf{n_{ji}}\right)\mathbf{p_j} - \frac{Z_0}{n_m}D_{ji}\mathbf{n_{ji}}\times\mathbf{m_j}\right]\\ \mathbf{H_{si,j}} &= \frac{e^{ikr_{ji}}}{4\pi r_{ji}}\left[\frac{Z_0}{\mu_0 n_m}D_{ji}\mathbf{n_{ji}}\times\mathbf{p_j} + \left(A_{ji}\mathbb{I}_3 + B_{ji}\mathbf{n_{ji}}\otimes\mathbf{n_{ji}}\right)\mathbf{m_j}\right]\end{aligned} \tag{2}$$

where n_m is the surrounding medium refractive index, k is the modulus of the wavevector ($k = 2\pi n_m/\lambda$), r_{ji} is the distance from the dipole j^{th} to the i^{th} dipole, ϵ_0 is the vacuum permittivity, $\mathbf{n_{ji}}$ is the unitary vector directed from the dipole j^{th} to the i^{th} dipole and Z_0 is the vacuum impedance. The following abbreviations were introduced

$$\begin{aligned}A_{ji} = A_{ij} &= k^2 - \frac{1}{r_{ij}^2} + \frac{ik}{r_{ij}}\\ B_{ji} = B_{ij} &= -k^2 + \frac{3}{r_{ij}^2} - \frac{3ik}{r_{ij}}\\ D_{ji} = D_{ij} &= k^2 + \frac{ik}{r_{ij}}\end{aligned} \tag{3}$$

If we now consider the case of N dipoles with general electric and magnetic dipolar moments as given by Eq. (1), the main problem will consist in obtaining the total local electromagnetic field, $(\mathbf{E_i}, \mathbf{H_i})$, at each dipole position. The i^{th} dipole is excited by a local field that is the superposition of the incident exciting wave and the field produced by the rest the dipoles obtained from summing Eq. (2) over all the dipoles surrounding the i^{th} one. The total local incident electromagnetic field in the i^{th} dipole can be written in the following way

$$\begin{pmatrix}\mathbf{E_i}\\ \mathbf{H_i}\end{pmatrix} = \sum_{j\neq i}\begin{pmatrix}\mathbf{E_{si,j}}\\ \mathbf{H_{si,j}}\end{pmatrix} + \begin{pmatrix}\mathbf{E_{inc,i}}\\ \mathbf{H_{inc,i}}\end{pmatrix} \tag{4}$$

where $\left(\mathbf{E_{inc,i}}, \mathbf{H_{inc,i}}\right)$ is the incident electromagnetic field of the exciting wave at the position of the i^{th} dipole.

From the coherent superposition of the radiated field by the N dipoles, a self-consistent system of $6N$ equations is obtained, where the $6N$ unknown variables are the three components of the electric and magnetic total local field at the N dipole positions (see Supplement 1, section S1). Any computing routine for the CDDA method should include two main parts once the position and polarizabilities of the N dipoles have been defined: one part should be able to define a $6N$ variable system of equations Eq. (4) that includes all the interactions between the dipoles as given by Eq. (2), and the other should be dedicated to solve the resulting system of $6N$ equations. Once the total local field in each dipole is known, it is straightforward to obtain the electric and magnetic dipole moments of each dipole through Eq. (1). Then the scattered field by each dipole can be obtained with Eq. (2), and then, the total field in the near- and far-field regimes can be obtained, by just summing the scattered field of each dipole.

2.2. Far field calculations: cross-sections

Here, we briefly introduce the equations used to calculate the absorption (σ_{abs}) and extinction cross sections (σ_{ext}). Assuming that the system of equations given by Eq. (4) has been solved, the

Optics EXPRESS

dipole moments at each dipole given by Eq. (1) can be obtained. Then, the following equations to obtain the extinction and absorption cross sections can be applied [45]

$$\begin{aligned}\sigma_{ext} &= \frac{k}{\epsilon_0 n_m^2 |E_0|^2} \sum_{i=1}^{N} \mathrm{Im}\left(\mathbf{E}^*_{\mathbf{inc,i}} \cdot \mathbf{p_i} + \mu_0 \mathbf{H}^*_{\mathbf{inc,i}} \cdot \mathbf{m_i}\right) \\ \sigma_{abs} &= \frac{k}{\epsilon_0 n_m^2 |E_0|^2} \sum_{i=1}^{N} \left[\mathrm{Im}\left(\mathbf{E}^*_{\mathbf{i}} \cdot \mathbf{p_i} + \mu_0 \mathbf{H}^*_{\mathbf{i}} \cdot \mathbf{m_i}\right) - \frac{k^3}{6\pi}\left(\frac{p_i^2}{\epsilon_0 n_m^2} + m_i^2\right)\right]\end{aligned} \tag{5}$$

where E_0 is the amplitude of the electric field of the incident wave.

The scattering cross section can be obtained as the difference between the extinction and absorption cross section, $\sigma_{sca} = \sigma_{ext} - \sigma_{abs}$. If the calculations are correctly implemented, this difference should be equal, within a certain numerical error, to the definition of scattering cross section [45]

$$\sigma_{sca} = \frac{k^2}{|E_0|^2} \int \left| \sum_{i=1}^{N} e^{-ikr_i} \left[(\mathbb{I}_3 - \mathbf{n} \otimes \mathbf{n}) \frac{\mathbf{p_i}}{\epsilon_0 n_m^2} - \frac{Z_0}{n_m} \mathbf{n} \times \mathbf{m_i} \right] \right|^2 d\Omega \tag{6}$$

A chiral system will produce different extinction for RCPL and LCPL, and its difference is known as CD. We will quantify the CD in terms of the difference between the extinction cross section for RCPL and LCPL

$$CD_{ext} \equiv \sigma_{ext,R} - \sigma_{ext,L} \tag{7}$$

where the subindexes R and L denote the RCPL and LCPL respectively. If CD is calculated in this way it will have cross section units (area).

Equation (5) enables handling the absorption and scattering contribution to the total extinction of each dipole independently, and this is a powerful tool to understand the origin of the resulting far-field spectra.

If we now consider the case of a single and weak dipolar scatterer, i.e. small polarizabilities as in the case of a realistic molecule, the absorption cross section of the molecule can be obtained. Due to the small size of molecules, extinction comes mainly from absorption [46]. By substituting Eq. (1) in Eq. (5) we obtain the expression of absorption cross section of a chiral molecule

$$\sigma_{ext} \approx \sigma_{abs} \approx \frac{k}{\epsilon_0 n_m^2 |E_0|^2} \left(\alpha''_{e,i} E_i^2 + \mu_0 \alpha''_{h,i} H_i^2 \mp \frac{4Z_0}{k n_m} \left| G''_i \right| C \right) \tag{8}$$

where the quotes in the polarizabilities indicate their imaginary part, the sign of the last term depends on the handedness of the molecule and C is the optical chirality density (OCD) defined as [44]

$$C = -\frac{n_m^2 \omega}{2c^2} \mathrm{Im}\left(\mathbf{E}^* \cdot \mathbf{H}\right) \tag{9}$$

This parameter has also a sign that depends on the handedness of the exciting light. RCPL and LCPL have opposite OCD signs. Calculating the difference between the RCPL and LCPL absorption cross sections with equation Eq. (8), it can be seen that only the last term contributes to that difference

$$CD_{abs} \equiv \sigma_{abs,R} - \sigma_{abs,L} = \mp \frac{8Z_0 \left| G''_i \right|}{\epsilon_0 n_m^3 |E_0|^2} C_R \tag{10}$$

where C_R is the OCD corresponding to the RCPL.

It can be concluded that the absorption CD of a chiral molecule is proportional to the OCD and its mixed magnetic-electric polarizability.

Optics EXPRESS

3. Validation of the method

We consider a case that can be analytically solved with the Mie theory. This consists of a sphere with two defined isotropic refractive indexes, one for RCPL and another LCPL, i.e. a sphere with circular birefringence. Such birefringence is characterized by a mixed magnetic-electric susceptibility χ_{eh}:

$$\begin{aligned} n_R &= n + \chi_{eh} \\ n_L &= n - \chi_{eh} \end{aligned} \tag{11}$$

where n is the mean refractive index, and R and L denote RCPL and LCPL respectively.

The problem of light scattering by spheres with isotropic circular birefringence is analytically solved in [46]. To solve the equivalent problem with CDDA we must derive the Clausius-Mossotti relations (CMR) for these systems (see Supplement 1, S2). We use this relation to describe the polarizability of the dipolar unit that is used to discretize the sphere. To derive the CMR relations, a bulk medium with analog constitutive relations as given in Eq. (1) are considered. For a non-magnetic medium, those relations are

$$\begin{aligned} \mathbf{P} &= \epsilon_0(n^2-1)\mathbf{E} - i\epsilon_0\chi_{eh}Z_0\mathbf{H} \\ \mathbf{M} &= i\frac{\chi_{eh}}{Z_0}\mathbf{E} \end{aligned} \tag{12}$$

By neglecting second or higher order terms in χ_{eh}, and considering vacuum as the surrounding medium, the electric and mixed magnetic-electric polarizability, $\alpha_{e,CM}$ and G_{CM} of a small unit cell of volume V inside such material can be expressed as

$$\begin{aligned} \alpha_{e,CM} &\approx 3V\frac{n^2-1}{n^2+2} \\ G_{CM} &\approx \frac{3V}{Z_0}\frac{\chi_{eh}}{n^2+2} \end{aligned} \tag{13}$$

Once the radius of the sphere and its refractive index are defined for LCPL and RCPL through the mixed magnetic-electric susceptibility, Mie exact calculation can be applied to obtain the

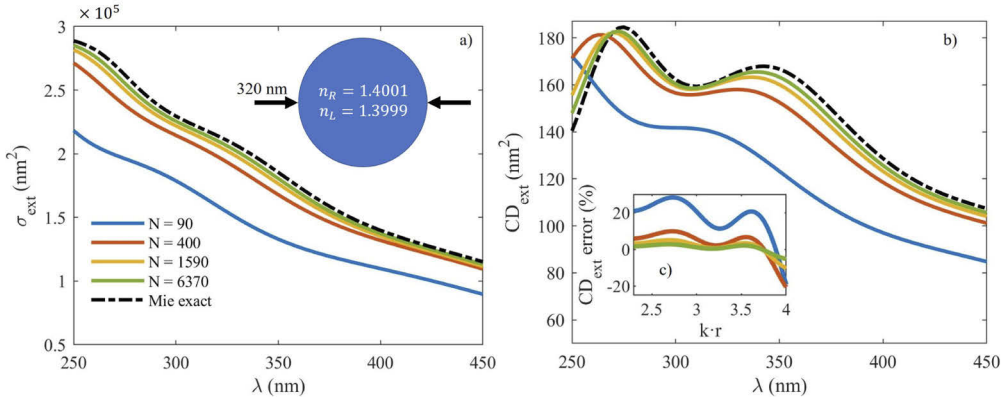

Fig. 1. Computation with the CDDA method of (a) the extinction cross section for RCPL, (b) extinction cross section dichroism (CD_{ext}) of a 160 nm diameter sphere with refractive index 1.4 and mixed magnetic-electric susceptibility of 10^{-4} considering a discretization of N dipoles (coloured solid lines). For comparison, the exact Mie calculation is also shown (black dashed). (c) Error in the extinction CD calculation compared to the exact Mie solution as a function of the size parameter.

Optics EXPRESS

solution used for comparison with the CDDA method. For the latter, we discretize the sphere in a large number of dipoles placed in a 3D cubic lattice. The polarizability of each dipole is that predicted by the Clausius-Mossotti relation in Eq. (13). A comparison between CDDA and exact Mie calculations is shown in Fig. 1 where a good agreement is obtained and can be further improved by increasing the number of discretizing dipoles. As shown in Fig. 1(c), the convergence is quite slow but not surprising since the cubic lattice is not efficient enough to describe the spherical surface of the sphere. Moreover, the radiative correction was only considered for the electric polarizability (see Supplement 1 S2). Apart from the polarizability description, the particle meshing can also be optimized. This is something important to consider in anisotropic and asymmetric nanoparticles [42].

4. Potential application of the CDDA method

Here, a simple but illustrative and relevant case will be analyzed with the CDDA method: the electromagnetic interaction between a spherical nanoparticle acting as a NA and a chiral 'pseudo-molecule': a small dipole that mimics the spectral response of a real molecule. A system that involves a finite number of molecules can be easily implemented in the CDDA method by just using dipolar polarizabilities that are straightforward to include in the calculations. Here, we show a comparison of the CD enhancement produced by two different spherical NAs interacting with a chiral molecule. One of the particles is made of silicon with a diameter of 125 nm and the other of gold with a diameter of 60 nm. These materials were chosen because they have been widely explored in experimental and theoretic studies [1–5,7–10,16,19,20,23,26]. However, this study is also applicable to other promising materials often employed in other spectral ranges, such as the UV, where Si and Au are not able to excite resonances [18,40]. As a first approach, the Au and Si nanospheres are described only by their effective magnetic-electric dipolar polarizabilities obtained from the Mie coefficients.

4.1. Dipolar description of the NA and the molecule

In this section, the polarizabilities of the NAs and the molecule are described. We used the optical constants given in the literature for Au [47] and Si [48]. The two first Mie coefficients, a_1 and b_1, were obtained from Mie theory once both, the radius and the optical properties of the surrounding medium (in this case water, $n_s = 1.33$) are defined [46]. The b_1 coefficient corresponds to the first resonance, the magnetic dipolar (MD) one, while the a_1 coefficient correspond to the second resonance, the electric dipolar (ED) one. Each resonance has an internal field distribution in the sphere that can be characterized through isotropic magnetic and electric dipolar moments whose polarizabilities are given by

$$\begin{aligned} \alpha_{e,s} &= i6\pi a_1/k^3 \\ \alpha_{h,s} &= i6\pi b_1/k^3 \end{aligned} \tag{14}$$

To describe the spectral features of the pseudo-molecule extinction, the Born-Kuhn model (BKM) [49] is employed. The BKM is a qualitative model that describes the main features of realistic molecules that due to their molecular structure have bonds that behave as coupled oscillators. In the BKM the spectral response is attributed to the resonance of two coupled and orthogonal electric dipoles. The resulting electric polarizability and the mixed magnetic-electric polarizability, in the limit of weak coupling oscillators and small size, can be expressed as

$$\begin{aligned} \alpha_e &= \frac{A}{\omega_0^2 - \omega^2 - i\gamma\omega} \\ G &= \frac{B\omega}{\omega_0^2 - \omega^2 - i\gamma\omega}\alpha_e \end{aligned} \tag{15}$$

Optics EXPRESS

where ω is the angular frequency, ω_0 is the resonant angular frequency, γ is the damping rate, and A and B are amplitude constants that depend on the probability of the optically induced molecular transition. For the sake of simplicity, the polarizabilities are assumed isotropic which could correspond to a mean value of all possible orientations of the molecule. It is straightforward to obtain reasonable values for ω_0, A, B and γ from some experimental measurements of biomolecules extinction [50–52]. Typically, the chiral part of the absorption due to G is very small, so its influence in the total extinction for any light polarization can be neglected. Usually, biomolecules show extinction resonances in the near UV, so the resonant frequency is typically $\omega_0 > 7 \times 10^{14}$ rad/s [50]. The value of A is chosen so that the peak value of the extinction cross section does not exceed 0.1 nm^2 [50–52] and the damping rate is directly related to the width of the resonance that can be obtained from the extinction spectrum, being typically in the order $0.1\omega_0$. Concerning B, it is non-zero only if the biomolecule exhibits a non-zero CD. From experimental measurements, the CD signal is typically 10^3 or 10^4 times smaller than the absorbance signal [51,52], thus the value of B is chosen to fulfill this requirement.

Figure 2 shows the extinction cross section and the CD spectrum of the pseudo-molecule obtained with the BKM. We can see two resonances slightly shifted in wavelength. One for RCPL and one for LCPL. This shift is mainly due to the coupling between the oscillators that models the molecule and is the origin of the CD. When these bonds are displayed in a completely non-symmetric way (breaking the mirror symmetry) like the two oscillators in the BKM, the molecule exhibits a CD. The degree of validity of this model is discussed in section S3 of the Supplement 1.

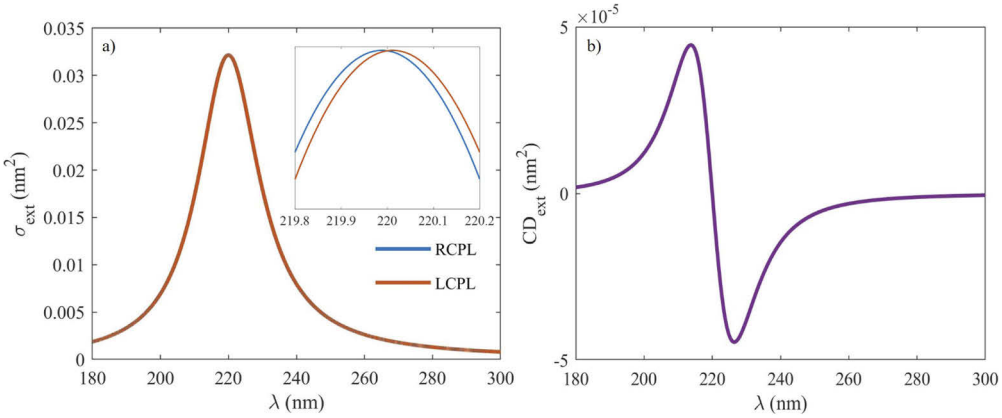

Fig. 2. (a) Extinction coefficient of the pseudo-molecule. The parameters of Eq. (15) were chosen ($\lambda_0 = 2\pi c/\omega_0 = 220$ nm, $\gamma = 0.1\omega_0$, $A = 10^{20}$ nm^{2}s^{-2}F and $B = 10^{20}$ nm^{-2}) so the values obtained for extinction and CD are realistic in base to the experimental bibliography. (b) CD of the pseudomolecule.

In Fig. 3 the extinction (blue), scattering (yellow) and absorption (red) cross section are shown for the Au and Si NAs. The electric near-field (NF) intensity (blue-yellow scale) and the OCD enhancement (blue-red scale) maps at the resonant wavelength ($\lambda = 540$ nm) are shown in the insets of their respective extinction spectrum. It can be seen that both, the 60 nm Au and 125 nm diameter Si NA exhibit a strong extinction resonance at the resonant wavelength. The Si NA size was chosen to make its MD resonance coincide with the purely ED of the Au NA resonance. This matching of resonances facilitates the comparison. We first point out the high extinction values of both NAs, being the Si NA extinction cross section more than 10 times larger than the Au one. This fact is in part due to the higher size of the Si NA, but also because its extinction efficiency is bigger [34]. Furthermore, it is important to note that the extinction for the Au NA

Optics EXPRESS

is mainly due to absorption while in the case of silicon is due to scattering. In both cases, the total extinction ($10^3 - 10^4$ nm^2) is several orders of magnitude larger than that of the molecule (0.01 nm^2). Therefore, we expect the molecule to generate a very small perturbation to the NA behavior when they interact. For Au, the 540 nm resonance comes mainly from the ED resonance, character while for the Si NA, at the same wavelength, the resonance has important contributions of both, the ED resonance (shorter wavelength) and the MD resonance (at 540 nm). In both cases, these resonances also imply a strong near-field enhancement that is typically exploited for surface-enhanced spectroscopies [34–37], including the CD enhancement of biomolecules [1–28].

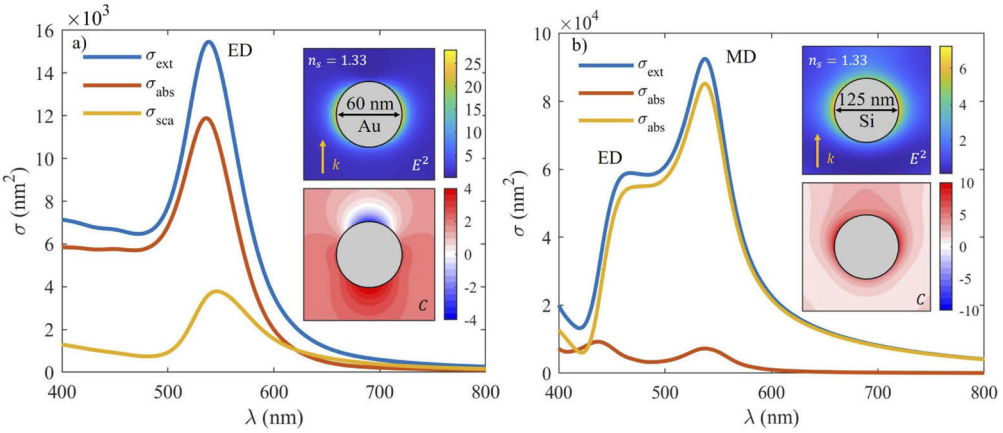

Fig. 3. Extinction (blue), absorption (red) and scattering (yellow) cross section of a 60 nm diameter gold (a) and 125 nm diameter silicon (b) NA. The insets with blue-yellow color map show the near electric field intensity distribution normalized to the incident plane wave electric field intensity. The insets with blue-red color-map show the OCD normalized to the values of the incident plane wave. All the insets are obtained for the main resonant wavelength of both materials, i.e. at 540 nm.

Concerning the insets of Fig. 3, it can be seen that the electric NF intensity of the Au NA is 4 times larger than that of the Si NA. This makes Au NAs efficient for surface enhanced spectroscopies (SERS, SEF, etc) where it is important to amplify the characteristic signal of the target. However, the absorption efficiency and thus the heat generation in Au are also larger. This characteristic could be an advantage for some thermal applications [53] but can also be a drawback in sensing applications where heating the sample can alter its response, destroy it or even melt the NA [54–56]. Silicon NAs, by contrast, offers the opportunity to compensate its lower NF intensity enhancement with its negligible absorption cross-section in the infrared range, where the molecules present their vibrational absorption bands. With near-zero absorption, it is possible to employ higher excitation powers in the near IR without destroying the sample the NA itself, making HRI NAs more efficient for sensing enhancement applications [34]. For the case of chiral sensing, which consist of detecting optical signals of chiral matter, in principle the electric field enhancement by itself is not enough to ensure a high CD signal. When molecular absorption is studied, the CD is proportional to the OCD [44] as discussed in section 2.2. Is in this parameter where HRI nanoparticles are generally better than metals [25]. This can be seen in the insets of Fig. 3 where the OCD enhancement (blue-red scale, C) of a Si NA is more than two-fold that of the Au one. Also, the spatial distribution (sign and magnitude) is uniform for the Si NA while this is not the case for the Au NA. This change of sign in C is also obtained in other metallic NAs like silver [25]. More information about the validity of the dipolar approximations of the NAs is given in the Supplement 1, S3.

Optics EXPRESS

4.2. Extinction CD enhancement

In this section, we calculate the optical response of the chiral molecule-NA system with the pseudo-molecule located at three different surface positions (top, 0, equator, $\pi/2$, and bottom, π) of the silicon and Au NAs. In experiments, direct measurements are based on extinction, for this reason the CD in terms of the extinction cross section (see Eq. (7)).

In Fig. 4(a) we show the extinction CD obtained for such interaction at those three positions. The greyish curves correspond to the molecule-Si NA interaction while the yellowish ones, correspond to the molecule-Au NA interaction. For comparison of the CD enhancement produced by the interactions of the molecule with each NA, the CD of the isolated molecule is shown with a purple solid line. In Fig. 4(b) the enhancement curves are shown. These were obtained by dividing the extinction CD obtained from the interactions by the extinction CD exhibited by the isolated molecule. In this part of the spectrum, the CD exhibited by the isolated molecule is very small (10^{-8}) as we are far from the molecule resonant wavelength (λ_0 = 220 nm). For the resonant wavelength of the NAs (540 nm), due to the interaction, the obtained CD signals are more than one order of magnitude higher, although still small compared signal generated by the isolated molecule in its absorption band. To obtain bigger signals, more than one molecule should be considered surrounding the NA or even a more sophisticated geometry for the NA should be optimized, but all these aspects are out of the scope of this work. With the Si NA we obtain a CD enhancement factor that varies from 45 to 70 depending on the relative position of the molecule. For the same wavelength, in the case of the gold NA, the CD sign changes depending on the position of the molecule, ranging from -15 to 20. In any case, the absolute value of the enhancement produced by the Au NA is smaller than those obtained with the Si NA. In both cases, the maximum enhancement is obtained when the molecule is placed at the NA equator. It is important to mention that, in general, the experimental situation is not the optimal one, but instead is an average of all possible relative positions. The reason is that the molecules are randomly distributed over the sphere. As a result, a colloid of a large number of NAs will cover almost every single possibility. It is clear to predict from Fig. 4 that the average enhancement of the Si NA will be larger than that of the gold NA for two main reasons: the gold NA exhibits lower absolute values and also shows a change of the sign of the CD enhancement factor.

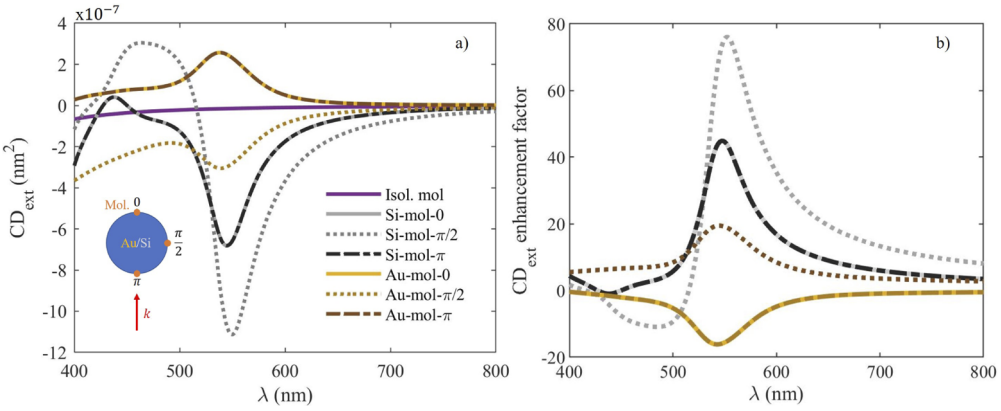

Fig. 4. (a) Extinction CD of the Au NA (yellowish curves) and the Si NA (greyish curves) with a molecule attached. Three locations for the molecule on the NA surface were considered: at the top (0) the equator ($\pi/2$) and the bottom (π) of the NA's surface. The purple curve is the Extinction CD exhibited by the isolated molecule. (b) Extinction CD of the NA with the molecule attached, normalized to the CD exhibited by the isolated molecule.

Optics EXPRESS

The OCD enhancements (see insets in Fig. 3) predict enhancement factors ([-4,4] for Au and [6,10] for Si) much lower than the ones observed in Fig. 4. The fact that the OCD enhancement in the near-field does not reproduce the measured far-field CD enhancement has been continuously evidenced in theoretical and experimental studies [1–6,24]. Many reasons have been proposed to explain it, but the mechanism of far-field CD enhancement is still unclear from a theoretical point of view. Here, we provide an approach to understand why the OCD enhancement shown in the near field is not enough to understand the far-field CD. The OCD calculations shown here and in related bibliography are always performed for the isolated nanostructure assuming that the molecule will not perturb the near-field distributions [17–20,40]. This is reasonable taking into account that molecules are indeed weak scatterers compared to NAs (see Fig. 2 and Fig. 3). This does not imply that there is no interaction between the NA and the molecule. The scattering of the sphere is perturbed by the presence of the molecule and therefore the extinction measurements in the far-field are affected by this near-field interaction [57]. In other words, in the far-field, we measure the extinction which is a sum of the scattering and absorption of both the molecule and the NA.

The OCD enhancement only predicts the absorption CD enhancement of the molecule (see Eq. (8)), but many more processes contribute to the measured extinction, for example, the scattering and absorption of the NA. To illustrate all these concepts, we apply the extinction theorem to the total system as in Fig. 4. In parallel, we apply it to the NA and the molecule separately to distinguish each contribution to the total extinction. In other words, we truncate the sum of the extinction cross section given in Eq. (5). This is one of the main advantages of the CDDA method, it allows the separation of each contribution to the total extinction, absorption, or even scattering in interaction problems. For simplicity, this study is focused on the optimal situation, i.e., when the molecule is in the equator, and only in terms of extinction. The result is shown in Fig. 5.

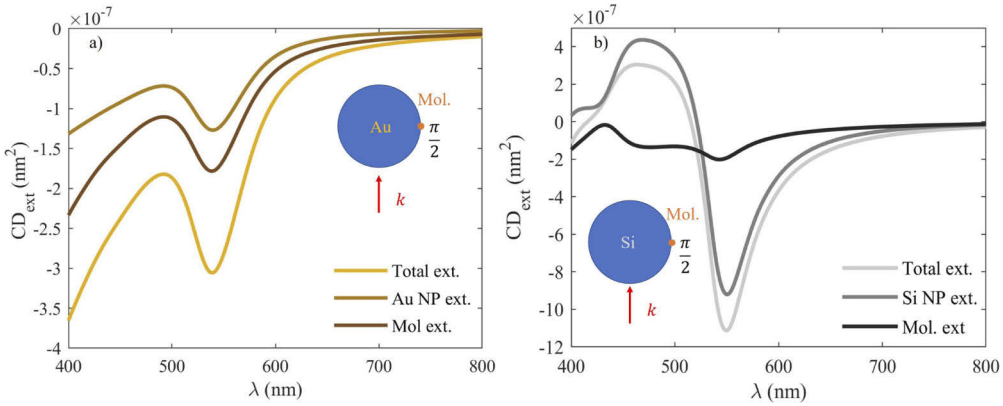

Fig. 5. Extinction CD of the molecule-NA system when the molecule is in the equator of the NA, for Au (a) and Si (b). The contribution of the molecule (darkest curves) and the NA (intermediate darkness) is independently calculated and compared to the total extinction (brightest curves).

It is clear that the contribution of the NA to the extinction CD is a very important part of the total CD. Noteworthy, the isolated sphere by itself does not generate any CD. The appearance of this CD comes strictly from its coupling to a chiral object, in this case, the chiral molecule. In fact, in the system molecule-Si NA, the main contribution to the CD is the scattering of the Si sphere while in the case of the Au is less important, although not negligible. This induced CD of a non-chiral object is not considered when predicting enhancements by modeling isolated achiral nanostructures. In those studies, the figure of merit for chiral sensing is only the OCD hot-spots

Optics EXPRESS

[17–20,40,44]. These OCD-hot spots are only relevant in two cases: when absorption dominates the extinction of the system, or when the study is centered in the separation of enantiomers using light absorption, e.g., different levels of ionization between left and right-handed enantiomers, enantioselective optical tweezers, etc $\cdots$ [18,20,58].

4.3. Absorption CD enhancement

In this section, the relevance of the OCD hot spots will be analyzed. The experimental measurement of molecular absorptions and in particular its separation from the whole extinction event is very difficult. However, the relevance of this process is crucial in the enantiomeric purification of racemic solutions [18,20]. In the same way, as the extinction CD contribution produced by the molecule was separated in Fig. 5, repeat it for the molecule's absorption as shown in Fig. 6. By studying the molecule's absorption cross section when interacting with the NA, the relevance of the OCD can be analyzed. The absorption CD of molecules interacting with NAs has been done before in the literature with other methods [4,8,26], but the direct relation with the OCD was not exposed. Under the dipolar approximation, the explicit derivation can be found in [25].

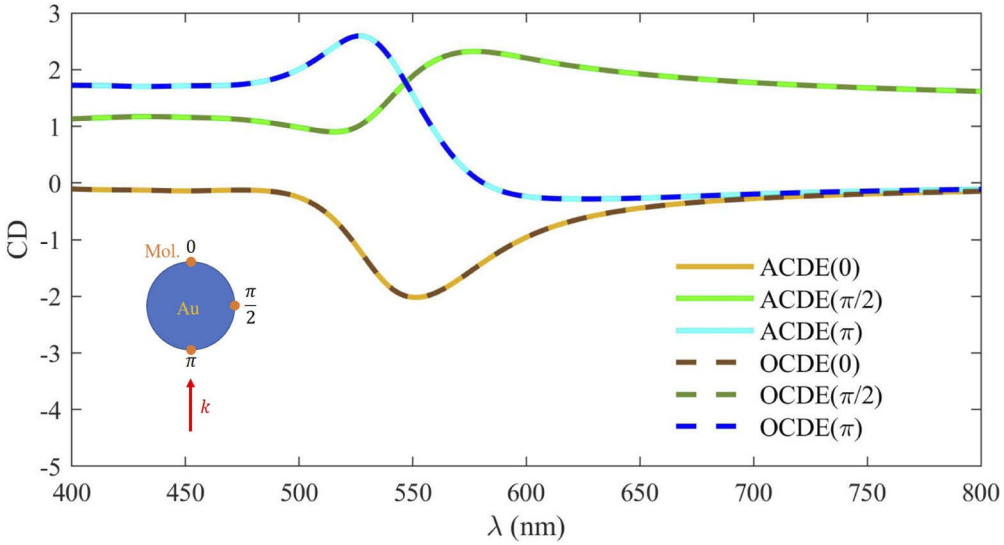

Fig. 6. Comparison of the absorption CD enhancement (ACDE) of the molecule contribution interacting with the Au NA (solid lines) and the near field OCD enhancement (OCDE) generated by the isolated sphere (dashed). These comparisons were done for the three positions indicated in the inset.

In Fig. 6, the molecule's absorption CD enhancement (ACDE) when interacting with the Au NA is plotted and compared to the near field OCD enhancement (OCDE) calculation of the isolated NA. We define the ACDE as the absorption CD exhibited by the molecule attached to the NA divided by the CD exhibited when it is isolated. For the ACDE calculation, the molecule is placed in three different positions over the surface of an Au NA, and then the OCDE produced by the isolated Au NA was calculated in those positions. It is important to note that we only take into account the contribution of the molecule absorption instead of the total absorption that includes the absorption of the nanoparticle. It can be seen, that the ACDE is the same as the OCDE in each point (dashed lines). This means that one can predict the ACDE of chiral molecules with the calculation of the OCD hot spots generated by isolated nanostructures. This was done to obtain the enhancement curves for Si and Ag spherical NAs in [25]. Therefore, it can be concluded that the absorption rate formula (Eq. (8)) only describes part of the physics of

Optics EXPRESS

the complete problem where also the sphere generates CD and this is not only due to absorption but also due to scattering. All these pieces together will give as a result a complex extinction CD spectrum that can only be described by considering the coupling phenomena as described in Fig. 4. Thanks to the easy handling of the contribution of each dipole in the extinction theorem, the CDDA allows understanding the physics of the CD enhancement.

4.4. Role of the magnetic and electric dipolar polarizability in the extinction CD

A significant advantage of the proposed CDDA method compared with others is the possibility of separating the MD-ED coherent superpositon terms that are responsible for CD enhancement. This facilitates the understanding of the physics behind the surface-enhanced CD in a particular problem where both kinds of resonances are present. As an illustrative example, the molecule-Si NA interaction was analyzed by introducing in our calculations artificial "switches" for the electric and magnetic dipolar polarizabilities of the Si NA. Figure 7 shows the resulting extinction spectra for each artificial "switch". Note that if one of the two polarizabilities is switched off, the peak values of the extinctions exhibit damping as each resonance has an important contribution to the other. To avoid misleading results, correcting factors were introduced to each polarizability, indicated in Fig. 7(a), for maintaining the peak values of the extinction constant.

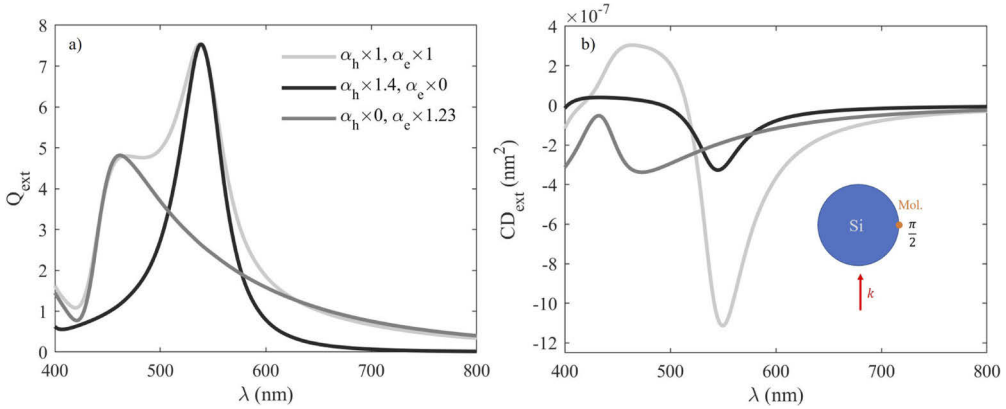

Fig. 7. (a) Extinction efficiency of isolated Si NA for the three studied situations:considering electric and magnetic polarizabilities (light gray), only magnetic polarizability (black), and only electric polarizability (darker gray). (b) Resulting extinction CD in those situations when the molecule is attached to the equator of the Si NA.

Figure 7(b) evidences the relevance of the simultaneous presence of both dipolar moments, magnetic and electric, in the interaction between the Si NA and a chiral molecule. In the cases where only one dipolar polarizability is present, either electric or magnetic, the enhancement of CD is weaker than the obtained in the case where both polarizabilities are present. In fact, in the pure electric or magnetic dipolar cases the enhancement is similar to the one obtained with the Au nanoparticle that only excites effectively an electric dipolar resonance. Therefore, CD in scattering is also enhanced due to the coherent superposition of ED and MD resonances, something that also happens with the OCD and thus the absorption CD [18,19,25].

5. Conclusions

In this research, we have introduced an extension to the DDA formalism where the effective polarizability of each dipole contains electric, magnetic and mixed magnetic-electric contributions, so that it can be used to solve light scattering problems in chiral systems. This mixed magnetic-electric polarizability is an inherent property of chiral substances like many biomolecules of interest in the pharmaceutical industry, where sensing chiral molecules in terms of CD is necessary.

Optics EXPRESS

In this sense, CDDA can help researchers to optimize the design of CD sensing devices based on nanostructures. Specifically, it helps to identify and individually control the different physical mechanisms involved in this problem in an easier way than other methods based on FEM or FDTD. To illustrate this, we have studied as representative case, the characterization of a chiral molecule in the presence of two different NA CD enhancers, one made of silicon and the other of gold. First, as expected, an achiral silicon NA interacting with a chiral molecule shows a higher CD signal enhancement. Second, we showed that most of the CD signal comes from the scattering of the NAs, usually much larger than molecules. From this, we conclude that the OCD hot spots generated by the NA in the near field only enhance the molecule absorption CD, which is only a small contribution to the total extinction. Finally, we have demonstrated the importance of the simultaneous presence of magnetic and electric dipolar moments in the NA to achieve optimal CD enhancement.

6. Abbreviations

- ACDE : absorption circular dichroism
- BKM : Born-Kuhn Model
- CDDA : chiral DDA
- CD : circular dichroism
- CMR : Clausius-Mossoti relation
- CPL : circularly polarized light
- DDA : discrete dipole approximation
- ED : electric dipolar
- FDTD: finite diferences in the time domain
- FEM : finite element method
- HRI : high refractive index
- LCPL : left circularly polarized light
- MD : magnetic dipolar
- NA : nanoantenna
- NF : near field
- OCD : optical chirality density
- OCDE : optical chirality density enhancement
- OR : optical rotation
- RCPL : right circularly polarized light
- SEF : surface enhanced fluorescence
- SERS : surface enhanced Raman

Funding. Ramon y Cajal Fellowship (RYC-2016- 20831); Ministerio de Educación, Cultura y Deporte (PGC2018-096649-B-I); Horizon 2020 Framework Programme (899598).

Optics EXPRESS

Disclosures. The authors declare no conflicts of interest.

Data availability. Data underlying the results presented in this paper are not publicly available at this time but may be obtained from the authors upon reasonable request.

Supplemental document. See Supplement 1 for supporting content.

References

1. J. García-Guirado, M. Svedendahl, J. Puigdollers, and R. Quidant, "Enhanced chiral sensing with dielectric nanoresonators," Nano Lett. **20**(1), 585–591 (2020).
2. B. M. Maoz, Y. Chaikin, A. B. Tesler, O. Bar Elli, Z. Fan, A. O. Govorov, and G. Markovich, "Amplification of chiroptical activity of chiral biomolecules by surface plasmons," Nano Lett. **13**(3), 1203–1209 (2013).
3. F. Lu, Y. Tian, M. Liu, D. Su, H. Zhang, A. O. Govorov, and O. Gang, "Discrete nanocubes as plasmonic reporters of molecular chirality," Nano Lett. **13**(7), 3145–3151 (2013).
4. J. M. Slocik, A. O. Govorov, and R. R. Naik, "Plasmonic circular dichroism of peptide-functionalized gold nanoparticles," Nano Lett. **11**(2), 701–705 (2011).
5. S. Yoo and Q.-H. Park, "Enhancement of chiroptical signals by circular differential mie scattering of nanoparticles," Sci. Rep. **5**(1), 14463 (2015).
6. Y. Guo, G. Zhu, and Y. Fang, "Plasmon–exciton coupling between plasmons and chiral molecules in core–shell structure under circularly polarized light excitation," J. Appl. Phys. **129**(4), 043104 (2021).
7. K. Yao and Y. Liu, "Enhancing circular dichroism by chiral hotspots in silicon nanocube dimers," Nanoscale **10**(18), 8779–8786 (2018).
8. S. Lee, S. Yoo, and Q.-H. Park, "Microscopic origin of surface-enhanced circular dichroism," ACS Photonics **4**(8), 2047–2052 (2017).
9. E. Mohammadi, K. L. Tsakmakidis, A. N. Askarpour, P. Dehkhoda, A. Tavakoli, and H. Altug, "Nanophotonic platforms for enhanced chiral sensing," ACS Photonics **5**(7), 2669–2675 (2018).
10. M. L. Nesterov, X. Yin, M. Schäferling, H. Giessen, and T. Weiss, "The role of plasmon-generated near fields for enhanced circular dichroism spectroscopy," ACS Photonics **3**(4), 578–583 (2016).
11. L. M. Kneer, E.-M. Roller, L. V. Besteiro, R. Schreiber, A. O. Govorov, and T. Liedl, "Circular dichroism of chiral molecules in dna-assembled plasmonic hotspots," ACS Nano **12**(9), 9110–9115 (2018).
12. V. Bochenkov and T. Shabatina, "Chiral plasmonic biosensors," Biosensors **8**(4), 120 (2018).
13. J. Kumar, K. G. Thomas, and L. M. Liz-Marzán, "Nanoscale chirality in metal and semiconductor nanoparticles," Chem. Commun. **52**(85), 12555–12569 (2016).
14. G. Shemer, O. Krichevski, G. Markovich, T. Molotsky, I. Lubitz, and A. B. Kotlyar, "Chirality of silver nanoparticles synthesized on DNA," J. Am. Chem. Soc. **128**(34), 11006–11007 (2006).
15. D. Vestler, A. Ben-Moshe, and G. Markovich, "Enhancement of circular dichroism of a chiral material by dielectric nanospheres," J. Phys. Chem. C **123**(8), 5017–5022 (2019).
16. N. A. Abdulrahman, Z. Fan, T. Tonooka, S. M. Kelly, N. Gadegaard, E. Hendry, A. O. Govorov, and M. Kadodwala, "Induced chirality through electromagnetic coupling between chiral molecular layers and plasmonic nanostructures," Nano Lett. **12**(2), 977–983 (2012).
17. F. R. Gomez, O. N. Oliveira Jr, P. Albella, and J. Mejia-Salazar, "Enhanced chiroptical activity with slotted high refractive index dielectric nanodisks," Phys. Rev. B **101**(15), 155403 (2020).
18. J. Hu, M. Lawrence, and J. A. Dionne, "High quality factor dielectric metasurfaces for ultraviolet circular dichroism spectroscopy," ACS Photonics **7**(1), 36–42 (2020).
19. M. L. Solomon, J. Hu, M. Lawrence, A. García-Etxarri, and J. A. Dionne, "Enantiospecific optical enhancement of chiral sensing and separation with dielectric metasurfaces," ACS Photonics **6**(1), 43–49 (2019).
20. C.-S. Ho, A. Garcia-Etxarri, Y. Zhao, and J. Dionne, "Enhancing enantioselective absorption using dielectric nanospheres," ACS Photonics **4**(2), 197–203 (2017).
21. X. Zhang, J. Yin, and J. Yoon, "Recent advances in development of chiral fluorescent and colorimetric sensors," Chem. Rev. **114**(9), 4918–4959 (2014).
22. Z. Fan and A. O. Govorov, "Plasmonic circular dichroism of chiral metal nanoparticle assemblies," Nano Lett. **10**(7), 2580–2587 (2010).
23. E. Mohammadi, A. Tittl, K. L. Tsakmakidis, T. V. Raziman, and A. G. Curto, "Dual nanoresonators for ultrasensitive chiral detection," ACS Photonics **8**(6), 1754–1762 (2021).
24. A. O. Govorov, Z. Fan, P. Hernandez, J. M. Slocik, and R. R. Naik, "Theory of circular dichroism of nanomaterials comprising chiral molecules and nanocrystals: Plasmon enhancement, dipole interactions, and dielectric effects," Nano Lett. **10**(4), 1374–1382 (2010).
25. A. García-Etxarri and J. A. Dionne, "Surface-enhanced circular dichroism spectroscopy mediated by nonchiral nanoantennas," Phys. Rev. B **87**(23), 235409 (2013).
26. T. Wu, R. Wang, and X. Zhang, "Plasmon-induced strong interaction between chiral molecules and orbital angular momentum of light," Sci. Rep. **5**(1), 18003 (2015).
27. T. J. Davis and D. E. Gómez, "Interaction of localized surface plasmons with chiral molecules," Phys. Rev. B **90**(23), 235424 (2014).

Optics EXPRESS

28. A. García-Etxarri, J. M. Ugalde, J. J. Sáenz, and V. Mujica, "Field-mediated chirality information transfer in molecule–nanoparticle hybrids," J. Phys. Chem. C **124**(2), 1560–1565 (2020).
29. N. M. Maier, P. Franco, and W. Lindner, "Separation of enantiomers: needs, challenges, perspectives," J. Chromatogr. A **906**(1-2), 3–33 (2001).
30. G. Balavoine, A. Moradpour, and H. B. Kagan, "Preparation of chiral compounds with high optical purity by irradiation with circularly polarized light, a model reaction for the prebiotic generation of optical activity," J. Am. Chem. Soc. **96**(16), 5152–5158 (1974).
31. P. Biagioni, J.-S. Huang, and B. Hecht, "Nanoantennas for visible and infrared radiation," Rep. Prog. Phys. **75**(2), 024402 (2012).
32. V. Giannini, A. I. Fernandez-Dominguez, S. C. Heck, and S. A. Maier, "Plasmonic nanoantennas: Fundamentals and their use in controlling the radiative properties of nanoemitters," Chem. Rev. **111**(6), 3888–3912 (2011).
33. I. Staude, T. Pertsch, and Y. S. Kivshar, "All-dielectric resonant meta-optics lightens up," ACS Photonics **6**(4), 802–814 (2019).
34. M. Caldarola, P. Albella, E. Cortés, M. Rahmani, T. Roschuk, G. Grinblat, R. F. Oulton, A. V. Bragas, and S. A. Maier, "Non-plasmonic nanoantennas for surface enhanced spectroscopies with ultra-low heat conversion," Nat. Commun. **6**(1), 7915 (2015).
35. P. Albella, M. A. Poyli, M. K. Schmidt, S. A. Maier, F. Moreno, J. J. Sáenz, and J. Aizpurua, "Low-loss electric and magnetic field-enhanced spectroscopy with subwavelength silicon dimers," J. Phys. Chem. C **117**(26), 13573–13584 (2013).
36. M. Moskovits, "Surface-enhanced spectroscopy," Rev. Mod. Phys. **57**(3), 783–826 (1985).
37. T. Vo-Dinh, "Surface-enhanced raman spectroscopy using metallic nanostructures," TrAC Trends Anal. Chem. **17**(8-9), 557–582 (1998).
38. M. Hentschel, M. Schäferling, X. Duan, H. Giessen, and N. Liu, "Chiral plasmonics," Sci. Adv. **3**(5), e1602735 (2017).
39. H.-E. Lee, H.-Y. Ahn, J. Mun, Y. Y. Lee, M. Kim, N. H. Cho, K. Chang, W. S. Kim, J. Rho, and K. T. Nam, "Amino-acid- and peptide-directed synthesis of chiral plasmonic gold nanoparticles," Nature **556**(7701), 360–365 (2018).
40. S. A. Rosales, F. González, F. Moreno, and Y. Gutiérrez, "Non-absorbing dielectric materials for surface-enhanced spectroscopies and chiral sensing in the uv," Nanomaterials **10**(10), 2078 (2020).
41. B. T. Draine and P. J. Flatau, "Discrete-dipole approximation for scattering calculations," J. Opt. Soc. Am. A **11**(4), 1491–1499 (1994).
42. M. A. Yurkin and A. G. Hoekstra, "The discrete-dipole-approximation code adda: capabilities and known limitations," J. Quant. Spectrosc. Radiat. Transfer **112**(13), 2234–2247 (2011).
43. G. W. Mulholland, C. F. Bohren, and K. A. Fuller, "Light scattering by agglomerates: Coupled electric and magnetic dipole method," Langmuir **10**(8), 2533–2546 (1994).
44. Y. Tang and A. E. Cohen, "Optical chirality and its interaction with matter," Phys. Rev. Lett. **104**(16), 163901 (2010).
45. P. C. Chaumet and A. Rahmani, "Coupled-dipole method for magnetic and negative-refraction materials," J. Quant. Spectrosc. Radiat. Transfer **110**(1-2), 22–29 (2009).
46. C. F. Bohren and D. R. Huffman, eds., *Absorption and Scattering of Light by Small Particles* (Wiley-VCH Verlag GmbH, Weinheim, Germany, 1998).
47. P. B. Johnson and R. W. Christy, "Optical constants of the noble metals," Phys. Rev. B **6**(12), 4370–4379 (1972).
48. E. Palik, ed., *Handbook of optical constants of solids* (Academic Press, California, USA, 1997).
49. M. Schäferling, "Chiral nanophotonics," Springer Ser. Opt. Sci. **205**, 159 (2017).
50. M. Taniguchi and J. S. Lindsey, "Database of absorption and fluorescence spectra of < 300 common compounds for use in photochemcad," Photochem. Photobiol. **94**, 290–327 (2018).
51. A. Bonvicini, L. Guilhaudis, V. Tognetti, D. Desmaële, N. Sauvonnet, H. Oulyadi, and L. Joubert, "Revisiting absorption and electronic circular dichroism spectra of cholesterol in solution: a joint experimental and theoretical study," Phys. Chem. Chem. Phys. **20**(7), 5274–5284 (2018).
52. N. Amdursky and M. M. Stevens, "Circular dichroism of amino acids: Following the structural formation of phenylalanine," ChemPhysChem **16**(13), 2768–2774 (2015).
53. G. Baffou and R. Quidant, "Thermo-plasmonics: using metallic nanostructures as nano-sources of heat," Laser Photonics Rev. **7**(2), 171–187 (2013).
54. M. Mahmoudi, S. E. Lohse, C. J. Murphy, A. Fathizadeh, A. Montazeri, and K. S. Suslick, "Variation of protein corona composition of gold nanoparticles following plasmonic heating," Nano Lett. **14**(1), 6–12 (2014).
55. A. Plech, V. Kotaidis, S. Grésillon, C. Dahmen, and G. Von Plessen, "Laser-induced heating and melting of gold nanoparticles studied by time-resolved x-ray scattering," Phys. Rev. B **70**(19), 195423 (2004).
56. M. D. King, S. Khadka, G. A. Craig, and M. D. Mason, "Effect of local heating on the sers efficiency of optically trapped prismatic nanoparticles," J. Phys. Chem. C **112**(31), 11751–11757 (2008).
57. P. Alonso-González, P. Albella, M. Schnell, J. Chen, F. Huth, A. García-Etxarri, F. Casanova, F. Golmar, L. Arzubiaga, L. Hueso, J. Aizpurua, and R. Hillenbrand, "Resolving the electromagnetic mechanism of surface-enhanced light scattering at single hot spots," Nat. Commun. **3**(1), 684 (2012).
58. Y. Zhao, A. A. Saleh, and J. A. Dionne, "Enantioselective optical trapping of chiral nanoparticles with plasmonic tweezers," ACS Photonics **3**(3), 304–309 (2016).